J. Fluid Mech. (2013), *vol.* 722, *pp.* 596–617.
doi:10.1017/jfm.2013.74

Turbulent flow in the bulk of Rayleigh–Bénard convection: small-scale properties in a cubic cell

Matthias Kaczorowski and Ke-Qing Xia†

Department of Physics, The Chinese University of Hong Kong, Shatin, Hong Kong, China

(Received 17 August 2012; revised 11 January 2013; accepted 30 January 2013;
first published online 28 March 2013)

The Rayleigh number (Ra) scaling of the global Bolgiano length scale $L_{B,global}$ and the local Bolgiano length scale $L_{B,centre}$ in the centre region of turbulent Rayleigh–Bénard convection are investigated for Prandtl numbers $Pr = 0.7$ and 4.38 and $3 \times 10^5 \leqslant Ra \leqslant 3 \times 10^9$. It is found that $L_{B,centre}$ does not necessarily exhibit the same scaling as $L_{B,global}$. While $L_{B,global}$ is monotonically deceasing as $L_{B,global} \sim Ra^{-0.10}$ for both Pr, $L_{B,centre}$ shows a steep increase beyond a certain Ra value. The complex scaling of the local Bolgiano length scale in the centre is a result of the different behaviour of the temperature-variance dissipation rate, ϵ_T, and the turbulent-kinetic-energy dissipation rate, ϵ_u. This shows that for sufficiently high Ra the flow is well-mixed and hence temperature is passively advected. It is also observed that the Ra-range in which $L_{B,centre}$ exhibits the same scaling as the global Bolgiano length scale is increasing with increasing Pr. It is further observed that for $Pr = 4.38$ and $Ra \leqslant 3 \times 10^7$ the local vertical heat flux in the centre region is balanced by the turbulent-kinetic-energy dissipation rate. For higher Ra we find that the local heat flux is decreasing. At $Pr = 0.7$ we do not observe such a balance, as the measured heat flux is between the heat fluxes estimated through the turbulent-kinetic-energy dissipation rate and the temperature-variance dissipation rate. We therefore suggest that the balance of the local heat flux might be Prandtl-number dependent. The conditional average of the local vertical heat flux $\langle Nu|\epsilon_u, \epsilon_T\rangle_{centre}$ in the core region of the flow reveals that the highest vertical heat flux occurs for rare events with very high dissipation rates, while the joint most probable dissipation rates are associated with very low values of vertical heat flux. It is also observed that high values of ϵ_u and ϵ_T tend to occur together. It is further observed that the longitudinal velocity structure functions approach Kolmogorov K41 scaling. The temperature structure functions appear to approach Bolgiano–Obukhov BO59 scaling for $r > L_{B,centre}$, while a scaling exponent smaller than the BO59 scaling is observed for separations $r < L_{B,centre}$. The mixed velocity and temperature structure function for $Ra = 1 \times 10^9$ and $Pr = 4.38$ shows a short 4/5-scaling for $r > L_{B,centre}$. Our results suggest that BO59 scaling might be more clearly observable at higher Prandtl and moderate Rayleigh numbers.

Key words: Bénard convection, isotropic turbulence, turbulent convection

† Email address for correspondence: kxia@phy.cuhk.edu.hk

1. Introduction

Thermally driven flows play an important role in many natural phenomena and technical applications, of which Rayleigh–Bénard convection (RBC) is a well-posed idealized system that allows the study of such flows. Despite the fact that this model system has been studied extensively (see e.g. Ahlers, Grossmann & Lohse 2009; Lohse & Xia 2010; Chillà & Schumacher 2012, for recent reviews), fundamental behaviours, such as whether or not the energy cascade exhibits a Bolgiano (1959) scaling in the inertial range are still debated, see e.g. Calzavarini, Toschi & Tripiccione (2002), Sun, Zhou & Xia (2006) and Kunnen *et al.* (2008).

In homogeneous and isotropic turbulence (HIT) and when the temperature is a passive scalar in the flow, the scalings of the velocity and temperature structure functions are expected to follow the Kolmogorov (K41) scaling (plus intermittency corrections). However, in thermally driven flows, the temperature cannot generally be considered passive. In such a case it is expected that the Bolgiano–Obukhov (BO59) scalings should apply above a certain length scale, called the Bolgiano length

$$L_B \equiv \epsilon_u^{5/4} \epsilon_T^{-3/4} (\alpha g)^{-3/2}. \tag{1.1}$$

Hence the inertial subrange is divided into two regions, $10\eta_k \lessapprox r < L_B$ and $L_B < r \ll L$, for which K41 and BO59 scalings apply, respectively, where L is the integral length scale of the system, and other variables are defined below.

In contrast to numerical simulations of HIT, which are typically based on forcing the flow at a certain (small range of) wavenumber(s), turbulent flow in the centre of RBC is a response to the imposed boundary conditions. The system is then determined by the Rayleigh number $Ra = \alpha g H^3 \Delta T/(\nu\kappa)$ and Prandtl number $Pr = \nu/\kappa$, where α, ν and κ are the thermal expansion coefficient, kinematic viscosity and thermal diffusivity, respectively, and g is the gravitational acceleration. The height of the fluid layer is given by H and the temperature difference between the horizontal top and bottom plates is ΔT.

It is generally believed that a BO59-like cascade should be observable in RBC at sufficiently high Ra, i.e. when Ra is sufficiently large to allow a long inertial subrange and the Bolgiano length scale L_B is sufficiently small to lie within the inertial range, since the globally averaged Bolgiano length scale can be written (in non-dimensional form) as

$$L_{B,global}/H = (Nu - 1)^{5/4} Nu^{-3/4} (RaPr)^{-1/4}, \tag{1.2}$$

which follows from averaging (1.1) over the entire volume and substituting the exact relations for the temperature-variance dissipation rate $\langle \epsilon_T \rangle_V = \kappa (\Delta T/H)^2 Nu$ and turbulent-kinetic-energy dissipation rate $\langle \epsilon_u \rangle_V = (Nu - 1)\nu^3 H^{-4} Pr^{-2} Ra$ obtained from the Boussinesq equations into it (see also Lohse & Xia 2010). Hence $L_{B,global} \sim Ra^{0.1}$ is readily obtained, when assuming an effective scaling $Nu \sim Ra^{0.3}$, which is a good approximation for the range of Ra considered here.

Velocity and temperature structure functions measured experimentally by Sun *et al.* (2006) and circulation structure functions measured by Zhou, Sun & Xia (2008) for $Ra \approx 10^{10}$ and $Pr = 4.4$ all follow the K41 prediction, rather than the BO59 prediction. This is also supported by direct numerical simulation (DNS) with shear-free horizontal boundaries (Calzavarini *et al.* 2002) at $Ra \approx 2 \times 10^7$ and $Pr = 1$. Being limited to low Ra, and hence an insufficiently long inertial range, the authors of the latter paper use the extended self-similarity (ESS) method to determine the inertial range and fitted it with a power law to determine the scaling exponent. Hence they show that BO59

scaling exists in the vicinity of the horizontal walls and scaling exponents of both temperature and velocity structure functions are close to K41 scaling in the centre.

However, numerical results obtained by Kunnen *et al.* (2008) extracted from the centre of their DNS at $Ra = 1 \times 10^8$ and $Pr = 4$ contradict this. Temperature structure functions in the radial direction and longitudinal structure functions of vertical velocity both show BO59 scaling above the Bolgiano length scale.

Recent numerical simulations of Rayleigh–Taylor turbulence by Boffetta *et al.* (2012) suggest that the lateral extent of the geometry might be a good means to confine the Bolgiano length scale, thus allowing one to study the transition from BO59-like to K41-like scaling of the structure functions. The geometrical confinement of the flow will, however, not be included here, but in a subsequent publication.

In this paper we use DNS of RBC in a cube in order to answer the question of how the local Bolgiano length scale varies with Ra for two different Prandtl numbers $Pr = 0.7$ and $Pr = 4.38$ and compare this scaling to the global estimate, in order to find out whether the global scaling can be applied to the bulk region. Furthermore, we extract the local heat flux in the centre of RBC and, analogously to Ni, Huang & Xia (2011), examine whether the local heat flux is balanced by the dissipation rate of turbulent kinetic energy or the temperature-variance dissipation rate, hence testing if their finding also applies to relatively low Prandtl numbers. Additionally, we investigate the joint probability density function (p.d.f.) of the two dissipation rates and examine the conditional average of the local vertical heat flux, depending on both dissipation rates, in order to gain a more complete picture of the heat transfer process in the bulk.

2. Set-up

2.1. *Numerical method*

The governing equations are solved in the Boussinesq approximation

$$\boldsymbol{\nabla} \cdot \boldsymbol{u} = 0, \tag{2.1a}$$

$$\partial \boldsymbol{u}/\partial t + \boldsymbol{u} \cdot \boldsymbol{\nabla} \boldsymbol{u} + \boldsymbol{\nabla} p = \nu \Delta \boldsymbol{u} + T \boldsymbol{e}_z, \tag{2.1b}$$

$$\partial T/\partial t + \boldsymbol{u} \cdot \boldsymbol{\nabla} T = \kappa \Delta T, \tag{2.1c}$$

where $\boldsymbol{u} = (u, v, w)$ is the velocity vector and T and p represent the temperature and pressure, respectively. The gravity vector is acting in the vertical direction, i.e. the $-\boldsymbol{e}_z$ direction. Equations (2.1) are discretized employing the finite volume method on non-equidistant Cartesian meshes with $N_x \times N_y \times N_z$ cells in the x-, y- and z-direction, respectively. Cell face values are approximated using fourth-order-accurate polynomials. The time integration is done using the Euler–leapfrog scheme, where the convective terms are discretized employing the leapfrog scheme and diffusive terms are discretized using Euler forward differencing. The solver is described in detail in Kaczorowski *et al.* (2008) and Shishkina, Shishkin & Wagner (2009).

Since the governing equations are solved in non-dimensional form using the normalizations $x_{ref} = H$, $u_{ref} = (\alpha g H \Delta T)^{1/2}$, $T_{ref} = \Delta T$ and $t_{ref} = x_{ref}/u_{ref}$, all results presented in the following are also non-dimensional, unless stated otherwise, i.e. they will be denoted with a hat ($\hat{\cdot}$).

2.2. *Computational set-up*

The geometry used here to study turbulent RBC is a cube bounded by solid walls at all boundaries, i.e. no-slip and impermeability conditions are applied to all walls. The sidewalls are adiabatic and the top and bottom plates isothermal. The Prandtl

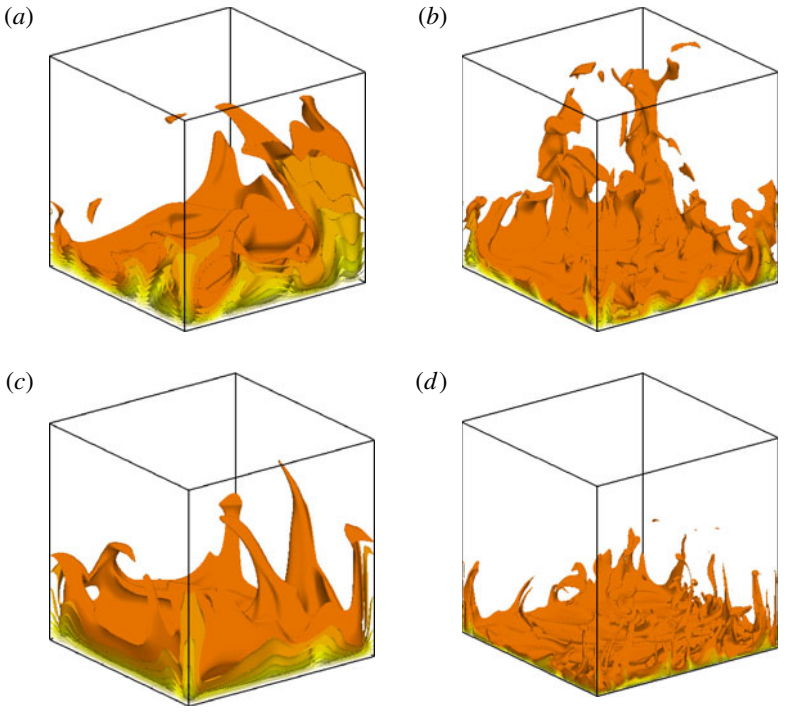

FIGURE 1. (Colour online) Visualization of the instantaneous temperature field with isosurfaces for $T \geqslant 0.1$ to give an impression of the size of the large coherent structures for different Ra and Pr: (*a*) $Ra = 1 \times 10^7$ and $Pr = 0.7$, (*b*) $Ra = 1 \times 10^8$ and $Pr = 0.7$, (*c*) $Ra = 1 \times 10^7$ and $Pr = 4.38$, (*d*) $Ra = 1 \times 10^9$ and $Pr = 4.38$.

numbers Pr under investigation are 0.7 and 4.38, representing the properties of the widely used media air at ambient conditions and water at 40 °C. An illustration of the isothermal surfaces formed by the flow at two different Ra for both Prandtl numbers is provided in figure 1, giving an impression of the size of the flow structures. The simulation parameters are summarized in table 1.

We designed the meshes such that the grid spacing in the bulk is smaller than the global estimate of the Kolmogorov and the Batchelor length scales. For $Ra \geqslant 2 \times 10^7$ ($Pr = 0.7$) and $Ra \geqslant 5 \times 10^7$ ($Pr = 4.38$) the grid spacing in the centre of the cell is equidistant as can be seen from figure 2(*a*). Towards the walls the grid spacing becomes finer in order to sufficiently resolve the boundary layers. For lower Ra the grid spacing is non-uniform throughout the cell.

It is noted that the resolution of the simulations exceeds the requirements proposed by Shishkina *et al.* (2010), so that all relevant turbulent scales should be resolved. In figure 2(*b*) a typical mesh and the resolution of the flow are shown for both Pr in order to provide evidence that the flow is sufficiently resolved – a necessity to obtain accurate results of small-scale quantities. It can be seen that the dissipative scales of turbulence are well-resolved in the bulk of the flow. However, it is also noted in passing that despite the fact that the resolution of the boundary layers for both Prandtl numbers is around twice the resolution requirement estimated by Shishkina *et al.* (2010), the boundary layers of the $Pr = 0.7$ simulations are not as well resolved as the resolution requirements might suggest.

Pr	Ra	$N_x \times N_y \times N_z$	N_H	N_T	N_v	Nu_S	Nu_{ϵ_T}	Nu_{ϵ_u}	t_{avg}
0.7	3×10^5	$64 \times 64 \times 64$	41	10/2.0	9/1.8	5.86	5.53	5.82	225
0.7	5×10^5	$64 \times 64 \times 64$	49	9/2.1	8/1.9	6.64	6.60	6.58	890
0.7	1×10^6	$82 \times 82 \times 82$	63	8/2.4	8/2.1	8.32	8.25	8.25	1080
0.7	2×10^6	$98 \times 98 \times 98$	78	7/2.6	6/2.3	10.1	10.0	10.0	900
0.7	3×10^6	$98 \times 98 \times 98$	89	6/2.8	5/2.5	11.5	11.3	11.4	760
0.7	5×10^6	$162 \times 162 \times 162$	106	9/3.0	8/2.6	13.6	13.4	13.4	710
0.7	1×10^7	$162 \times 162 \times 162$	132	7/3.3	7/2.9	16.3	16.1	16.2	390
0.7	2×10^7	$194 \times 194 \times 194$	165	8/3.7	7/3.2	19.6	19.5	19.7	200
0.7	3×10^7	$290 \times 290 \times 290$	191	10/3.9	9/3.4	22.0	22.0	22.1	308
0.7	1×10^8	$290 \times 290 \times 290$	281	7/4.6	6/4.1	31.3	31.1	31.8	300
4.38	1×10^6	$64 \times 64 \times 64$	52	7/1.9	9/3.2	8.35	8.22	8.28	300
4.38	5×10^6	$178 \times 178 \times 194$	88	17/2.4	25/4.0	13.1	13.1	13.1	400
4.38	8×10^6	$178 \times 178 \times 194$	103	15/2.6	22/4.32	15.4	15.4	15.3	530
4.38	1×10^7	$178 \times 178 \times 194$	110	14/2.6	21/4.5	16.1	16.0	16.1	520
4.38	3×10^7	$242 \times 242 \times 258$	160	11/3.2	17/5.3	22.6	22.4	22.3	570
4.38	5×10^7	$258 \times 258 \times 258$	189	7/3.4	12/5.7	26.2	26.2	26.3	375
4.38	1×10^8	$258 \times 258 \times 258$	236	6/3.8	10/6.3	32.2	31.7	32.0	750
4.38	2×10^8	$354 \times 354 \times 354$	295	7/4.1	11/6.9	39.3	38.9	39.2	625
4.38	3×10^8	$354 \times 354 \times 354$	338	7/4.4	10/7.4	44.4	43.8	44.3	525
4.38	1×10^9	$514 \times 514 \times 514$	501	13/5.3	19/8.8	63.4	62.7	63.0	350
4.38	3×10^9	$770 \times 770 \times 770$	719	13/6.3	19/10.4	88.3	89.6	89.4	90

TABLE 1. Simulation parameters and mean heat flux. The number of grid points $N_x \times N_y \times N_z$ in the respective spatial direction; required number of grid points N_H in the vertical direction; number of grid points required for resolving the thermal N_T and the viscous N_v boundary layers (actual resolution/requirement); mean heat transfer Nu_S calculated in horizontal slices, $Nu_{\epsilon_T} = (RaPr)^{1/2} \langle \epsilon_T \rangle_{global}$ and $Nu_{\epsilon_u} = (RaPr)^{1/2} \langle \epsilon_u \rangle_{global} + 1$. t_{avg} denotes the averaging time of the simulations in free-fall time units.

We also checked the bulk resolution by investigating the scaling of the second-order longitudinal and transverse structure functions, $S_2^{w_l}$ and $S_2^{w_t}$, of vertical velocity fluctuations w' with separations r in the dissipative range. The velocity increments in the centre of the cell have been averaged spatially over a volume $V_{centre} = (0.5H)^3$. From figure 3 it can be seen that $S_2^{w_l}(r) = S_2^{w_t}(r)/2$, where $S_2^{w_l}(r) = \langle (w'(\boldsymbol{r}_0 + r\boldsymbol{e}_z) - w'(\boldsymbol{r}_0))^2 \rangle_{t,centre} \sim r^2$ and $S_2^{w_t}(r) = \langle (w'(\boldsymbol{r}_0 + r\boldsymbol{e}_x) - w'(\boldsymbol{r}_0))^2 \rangle_{t,centre} \sim r^2$, when r is of the order of the Kolmogorov length scale or smaller. On the one hand this proves that the bulk resolution is sufficient to resolve the dissipative scales of the flow, on the other hand it also shows that the bulk turbulence at these Rayleigh numbers is homogeneous and isotropic.

In order to verify the global properties obtained from our simulations, we compare the Nusselt number with numerical and experimental results from the literature. Figure 4 reveals that our data for $Pr = 4.38$ match the experimental measurement by Funfschilling *et al.* (2005) obtained in a cylindrical cell with $Pr = 4.4$ and aspect ratio unity very well. For moderate Ra ($10^7 \lessapprox Ra \lessapprox 10^9$) our Nu-data for $Pr = 0.7$ are roughly 2 % lower than for the higher Prandtl number case. The observation that the Nusselt number at a Prandtl number of 0.7 is lower than at a Prandtl number of 4.4 matches the extrapolation of the experimental observation of Xia, Lam & Zhou (2002), who observed that the Prandtl number dependence of the heat flux exhibits a maximum around a Prandtl number of 4–6. However, comparing the results by

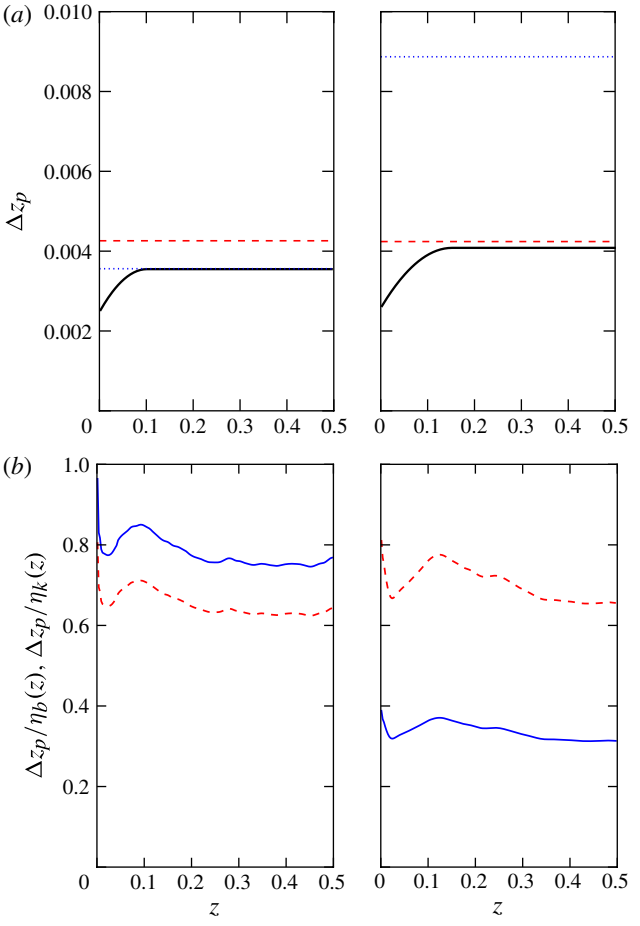

FIGURE 2. (Colour online) (*a*) Grid spacing in the vertical direction of the cube (—) compared with global estimates for the Kolmogorov (···) and Batchelor (- -) length scale for $Ra = 1 \times 10^8$ and $Pr = 0.7$ (left) and for $Ra = 1 \times 10^8$ and $Pr = 4.38$ (right). (*b*) The grid spacing in terms of the Kolmogorov (—) and Batchelor length scales (- -) for the same configuration as in (*a*). For symmetry reasons only half of each profile is shown.

Wagner, Shishkina & Wagner (2012) obtained in cylindrical cells with $Pr \approx 0.7$ with the experiments by Funfschilling *et al.* (2005) suggests that there is no difference in the Nusselt number between those Prandtl numbers. In terms of scaling both of our data sets are close to the results by Funfschilling *et al.* (2005) and Wagner *et al.* (2012), which both used a geometry with aspect ratio one.

3. Profiles of the local Bolgiano length scale

It is known (Benzi, Toschi & Tripiccione 1998; Kunnen *et al.* 2008) that the local Bolgiano length scale L_B depends on the position in the convection cell, where small L_B values are found near the isothermal plates and large ones near the adiabatic sidewall, reflecting the different boundary conditions of the respective walls. In terms of our set of normalized variables the local Bolgiano length scale defined in (1.1) can

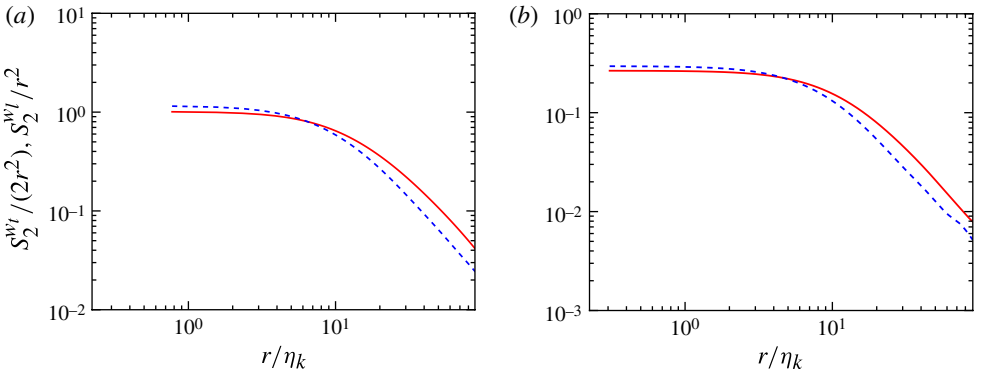

FIGURE 3. (Colour online) Comparison of the second-order transverse structure function S_2^{wt} (- -) with the second-order longitudinal structure function S_2^{wl} (—) plotted in compensated form for (*a*) $Ra = 1 \times 10^8$, $Pr = 0.7$ and (*b*) $Ra = 3 \times 10^9$, $Pr = 4.38$.

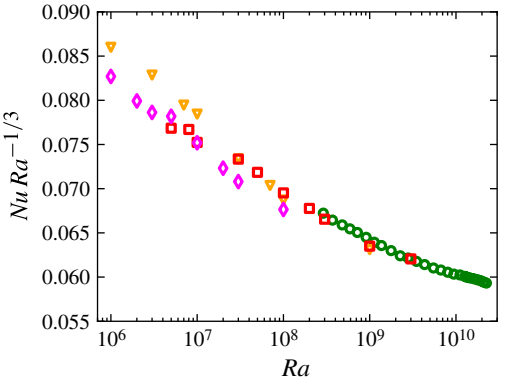

FIGURE 4. (Colour online) *Nu–Ra* relation in the cube for $Pr = 0.7$ (◊) and $Pr = 4.38$ (□). For comparison results obtained in cylindrical geometries using DNS with $Pr = 0.786$ and aspect ratio unity by Wagner *et al.* (2012) (▽), and experimental measurements with $Pr = 4.4$ and aspect ratio unity by Funfschilling *et al.* (2005) (○) are also shown.

be calculated as

$$L_B(x, y, z) = \langle \epsilon_u\,(x, y, z)^{5/4} \rangle_t \, \langle \epsilon_T\,(x, y, z)^{-3/4} \rangle_t, \tag{3.1}$$

where $\langle \epsilon_T(x, y, z) \rangle_t = (RaPr)^{-1/2} \, \langle \sum_i (\partial T'/\partial x_i)^2 \rangle_t$ is the non-dimensional time-averaged temperature-variance dissipation rate, $\langle \epsilon_u(x, y, z) \rangle_t = (Ra/Pr)^{-1/2} \, \langle \sum_i \sum_j (\partial u_i'/\partial x_j)^2 \rangle_t$ the non-dimensional time-averaged turbulent-kinetic-energy dissipation rate and primed quantities denote turbulent fluctuations. Averaging the local Bolgiano length scale $L_B(x, y, z)$ in space, one obtains the mean of the local Bolgiano length scales, which is then given by $\langle L_B(x, y, z) \rangle_{\delta V} = \langle \langle \epsilon_u\,(x, y, z)^{5/4} \rangle_t \, \langle \epsilon_T\,(x, y, z)^{-3/4} \rangle_t \rangle_{\delta V}$, where δV denotes the averaging volume. In the present paper we shall, however, evaluate the structure functions averaged over the bulk region, so that the mean Bolgiano length scale is defined as

$$L_{B,centre} = \langle \epsilon_u \rangle_{centre,t}^{5/4} \, \langle \epsilon_T \rangle_{centre,t}^{-3/4}, \tag{3.2}$$

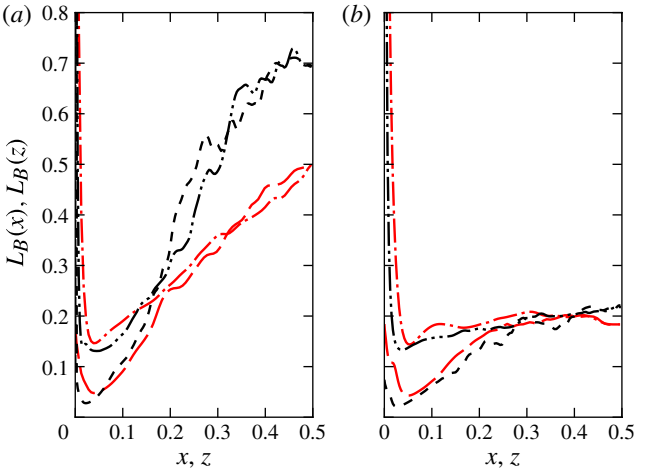

FIGURE 5. (Colour online) Time-averaged profiles of the local Bolgiano length scale through the centre of the cube $L_B(x) = L_B(x, y = 0.5, z = 0.5)$ and $L_B(z) = L_B(x = 0.5, y = 0.5, z)$ for (*a*) $Pr = 0.7$ and (*b*) $Pr = 4.38$. Plotted are profiles for $Ra = 1 \times 10^7$ in the vertical (– –) and the horizontal (- · -) direction and for $Ra = 1 \times 10^8$ in the vertical (- -) and the horizontal (- · · -) direction. For symmetry reasons only half of each profile is shown.

which follows from equating (6.1) and (6.3) or (6.2) and (6.4) (see § 6 below) and consequently results in the mean Bolgiano length scale of the bulk region being a function of $\langle \epsilon_u \rangle_{centre,t}$ and $\langle \epsilon_T \rangle_{centre,t}$, since the structure functions are averaged over the bulk region.

In figure 5 profiles of L_B for $Pr = 0.7$ and 4.38 measured locally through the centre of the cube illustrate the strong influence of the Prandtl number on the Bolgiano length scale in the centre of the cell. Due to the symmetry of the flow we only plot half of the profile, from the wall at $x = 0$ (sidewall) or $z = 0$ (hot bottom plate) to the centre of the cell at $x, z = 0.5$. The profile in figure 5(*a*) shows the familiar shape of the L_B-profile already shown by Benzi *et al.* (1998). However, we note that despite the similar values of $Ra \approx 10^7$ and $Pr \approx 1$, the local Bolgiano length scale in the centre of the cell in the present simulations is only $\sim 1/3$ of the one observed by Benzi *et al.* (1998). Since the simulation parameters are essentially the same, the only remaining difference is that Benzi *et al.* (1998) use slip boundary conditions on the horizontal plates and periodic boundary conditions in the horizontal directions, while no-slip conditions are employed on all walls of our simulations. We therefore infer that the dynamics of the core region are significantly influenced by the boundary conditions, and hence the dynamics of the adjacent boundary layers.

It can also be seen from figure 5 that due to the different boundary conditions in the horizontal and the vertical direction $L_B(x)$ and $L_B(z)$ show a different behaviour outside the core region. In the subsequent sections we therefore evaluate the turbulent properties of the flow in a region $3/8 \leqslant x, y, z \leqslant 5/8$, where we can assume similar properties of the flow in both the horizontal and the vertical direction.

A comparison of figures 5(*a*) and 5(*b*) also demonstrates that the Prandtl number dependence of the local Bolgiano length scale is a function of Ra. While $L_B(x, z)$ in the bulk does not change significantly from $Ra = 1 \times 10^7$ to 1×10^8 when $Pr = 4.38$, it increases dramatically for $Pr = 0.7$, while the global Bolgiano length scale is

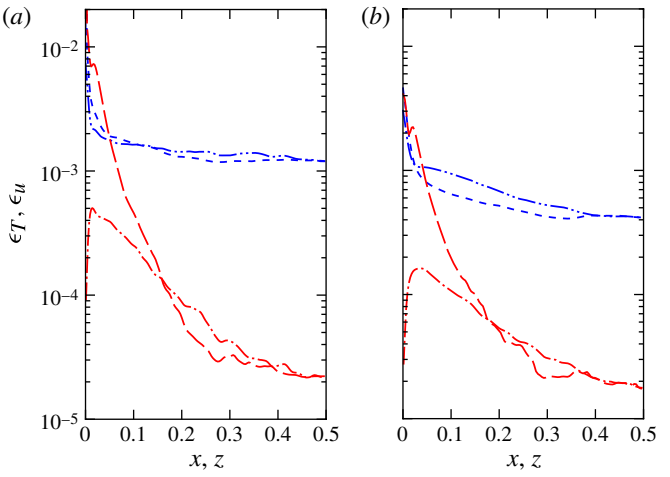

FIGURE 6. (Colour online) Profiles of the turbulent-kinetic-energy dissipation rate in the vertical (- -) and the horizontal directions (– ·· –) and temperature-variance dissipation rate in the vertical (– –) and the horizontal directions (– · –) for $Ra = 1 \times 10^8$ through the centre of the cube. For symmetry reasons only half of each profile is shown.

decreasing for both Pr. Hence the behaviour of the local Bolgiano length scale can be entirely different from the globally averaged Bolgiano length scale.

Since both ϵ_u and ϵ_T contribute to the Bolgiano length scale, it is interesting to ask where the different behaviour of the L_B-profiles comes from: a change of the temperature-variance dissipation rate or a change of the turbulent-kinetic-energy dissipation rate? Figure 6 reveals that the profiles of ϵ_T, both in the horizontal and the vertical direction are very similar for both Prandtl number cases, while the ϵ_u profiles are very similar in shape, but their absolute values differ by about one order of magnitude. The higher energy dissipation rate for $Pr = 0.7$ thus leads to a significantly larger Bolgiano length scale.

4. *Ra*-scaling of the flow

A plot of the Bolgiano length scale against Rayleigh number averaged both locally for a volume $V_{centre} = (0.25H)^3$ as described above and globally calculated by (1.2) for $Pr = 0.7$ and 4.38 presented in figure 7 illustrates the power-law decrease of $L_{B,global}$ and the complex Ra-scaling of $L_{B,centre}$. A least-squares fit of the globally averaged Bolgiano length scales yields $L_{B,global}(Pr = 0.7) = 0.420\,Ra^{-0.104}$ and $L_{B,global}(Pr = 4.38) = 0.251\,Ra^{-0.101}$. For $Pr = 4.38$ and moderate Ra the scaling of the local and global Bolgiano length scale are identical, whereas for $Ra < 1 \times 10^7$ and $Ra > 2 \times 10^8$ the scalings differ, i.e. $L_{B,centre}$ increases with Ra, and hence behaves contrary to the globally averaged Bolgiano length scale. Kunnen *et al.* (2008) have investigated the global and local Bolgiano length scale in a cylindrical container using DNS. Here we compare our data to their results obtained for $Pr = 4$, which is in the range $1 \times 10^8 \leqslant Ra \leqslant 1 \times 10^{10}$. Before investigating the scaling of the local Bolgiano length scale in the centre of the cell, we deduce from figure 1(*b*) of their paper that both the turbulent-kinetic-energy dissipation rate and the temperature-variance dissipation rate for $Ra = 1 \times 10^9$ and $Pr = 6.4$ match the experimental data by He *et al.* (2007) and Ni *et al.* (2011) closely. The Bolgiano length scale extracted from the centre of their

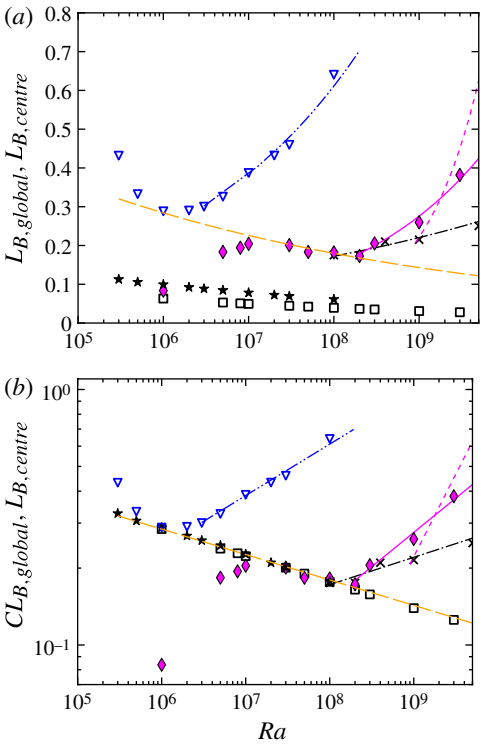

FIGURE 7. (Colour online) (*a*) Ra-scaling of the local Bolgiano length scale $L_{B,centre}$ averaged over a volume $V_{centre} = (0.25H)^3$. (*b*) Log–log plot of the globally averaged Bolgiano length scales together with their least-squares fits $L_{B,global}(Pr = 0.7) = 0.420\,Ra^{-0.104}$ and $L_{B,global}(Pr = 4.38) = 0.251\,Ra^{-0.101}$. The global Bolgiano scales have been multiplied by $C(Pr = 0.7) = 3.3$ and $C(Pr = 4.38) = 5.0$ to allow a better comparison of the scaling of local and global scales. $Pr = 0.7$ ($\triangledown$) and $Pr = 4.38$ ($\blacklozenge$) and the respective global Bolgiano length scale $L_{B,global}$ for $Pr = 0.7$ ($\star$) and $Pr = 4.38$ ($\square$). The least-squares fit $\langle L_B \rangle_{centre} = 0.024\,Ra^{0.107}$ (-·-) obtained from DNS by Kunnen *et al.* (2008) for $Pr = 4$ and the corresponding data points ($\times$) are given for reference. The long-dashed line represents the least-squares fit $L_{B,centre} = 1.123Ra^{-0.10}$ to the data of both Prandtl numbers that scales similarly to the global length scale. The least-squares fits $L_{B,centre} = 0.020 \times Ra^{0.18}$ (– ·· –) for $Pr = 0.7$ and $L_{B,centre} = 6.79 \times 10^{-4}Ra^{0.29}$ (—) for $Pr = 4.38$ are given for reference. Additionally the scaling of the local Bolgiano length scale in the centre computed from the scalings $\epsilon_u \sim Ra^{0.02}$ (Ni *et al.* 2011) and $\epsilon_T \sim Ra^{-0.83}$ (He, Tong & Xia 2007) is provided (- -).

cylindrical cell is in excellent agreement with our data for $Ra \leqslant 3 \times 10^8$, but differs significantly for $Ra > 3 \times 10^8$. However, their Bolgiano length scale in the bulk is calculated in a different way from ours, i.e. using (3.1), while we are using (3.2). A direct comparison of the L_B–Ra-scaling of Kunnen *et al.* (2008) and our data is therefore not possible. A comparison of the local Bolgiano length scale in a cubic and a cylindrical cell is, however, possible by using the experimental data by He *et al.* (2007) and Ni *et al.* (2011) to calculate the scaling of L_B in the bulk. This yields $L_{B,centre} = 3.47 \times 10^{-7}Ra^{0.645}$, when using the offset scaling of ϵ_T, whose multiplicative constant is adjusted to our DNS data. Had we used the data by He *et al.* (2007)

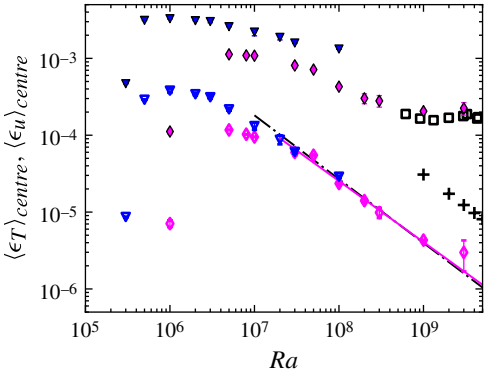

FIGURE 8. (Colour online) Ra-scaling of the turbulent-kinetic-energy and temperature-variance dissipation rate for $Pr = 0.7$ (ϵ_u: ▼; ϵ_T: ▽) and $Pr = 4.38$ (ϵ_u: ♦; ϵ_T: ◊). The error bars are calculated from the difference between the average of the entire time series and the second half of it. The solid line represents the least-squares fit $\epsilon_T = 44.58Ra^{-0.78}$. For reference experimental measurements of ϵ_T (+) by He *et al.* (2007) and of ϵ_u (□) by Ni *et al.* (2011), both in the centre of the cell, are plotted. Both experiments were conducted in water with $Pr \approx 4.4$. For comparison the scaling $\epsilon_T \sim Ra^{-0.83}$ (-·-) obtained by He *et al.* (2007) is shifted towards the numerical data. Note that the normalization used here differs from the one used by He *et al.* (2007) in their paper – see text for more details..

directly without offset, the resulting L_B would be only 20 % of the value plotted in figure 7.

A generally similar behaviour of the local Bolgiano length scale is observed for $Pr = 0.7$; however, the transition to a rapid increase with Ra in this case has already occurred at $Ra \approx 3 \times 10^6$. Least-squares fits to the region where $L_{B,centre}$ is rapidly increasing yield $L_{B,centre} = 0.020 \times Ra^{0.18}$ for $Pr = 0.7$ and $L_{B,centre} = 6.79 \times 10^{-4} Ra^{0.29}$ for $Pr = 4.38$.

The complex dynamics of the flow in the core region therefore do not necessarily allow an application of the scaling of (1.2) to the core region, if Ra is either too large or too small, where the range of validity strongly depends on Pr. Analysis of the corresponding turbulent-kinetic-energy dissipation rate and temperature-variance dissipation rate shown in figure 8 reveals that the Ra-scalings of ϵ_T and ϵ_u exhibit a different behaviour. While the scaling of ϵ_u shows a clear Prandtl number dependence and approaches a plateau for sufficiently high Ra, the scaling of ϵ_T does not show a Prandtl number dependence for high Ra ($Ra > 3 \times 10^7$ for the Prandtl numbers studied here) and follows the scaling $\epsilon_T \sim Ra^{-0.78}$.

The values of ϵ_u match the experimental data by Ni *et al.* (2011) measured in the centre of a cylindrical cell. He *et al.* (2007) experimentally measured the temperature-variance dissipation rate in the range $1 \times 10^9 \leqslant Ra \leqslant 1 \times 10^{10}$ and obtained the scaling $\hat{\epsilon}_T/(\hat{\kappa}\,(\Delta\hat{T}/\hat{H})^2) = 2.9 \times Ra^{-0.33}$ in the centre of their water-filled cell. Using the normalization introduced in § 2.1 yields $\epsilon_T = 2.9 Pr^{-1/2} \times Ra^{-0.83}$ for the experimentally measured results (the normalized temperature-variance dissipation rate satisfies the relation $\hat{\epsilon}_T = \hat{\kappa}\,(\Delta\hat{T}/\hat{H})^2\,(RaPr)^{1/2}\,\epsilon_T$ and the normalized kinetic-energy dissipation rate satisfies $\hat{\epsilon}_u = \hat{\nu}^3\hat{H}^{-4}\,(Ra/Pr)^{-3/2}\,\epsilon_u$). For $5 \times 10^7 \leqslant Ra \leqslant 1 \times 10^9$ and $Pr = 4.38$ we obtain the scaling of the temperature-variance dissipation rate $\epsilon_T = 43.9 \times Ra^{-0.78}$. While the scaling exponents of experiment and DNS match very well, the magnitude

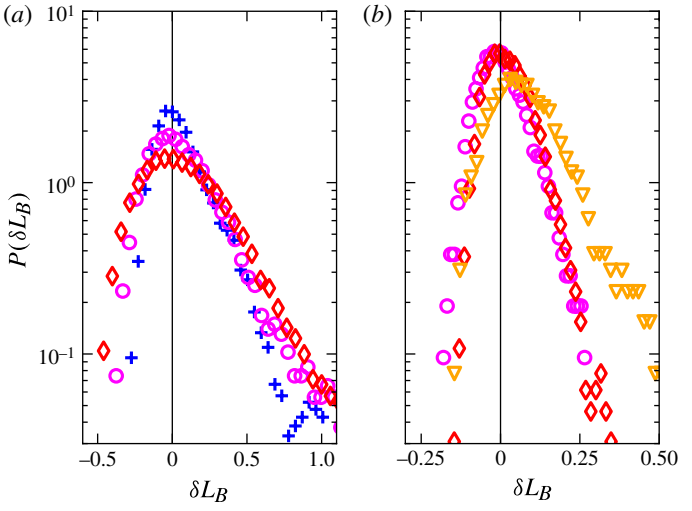

FIGURE 9. (Colour online) p.d.f.s of the Bolgiano length scale differences $\delta L_B = L_{B,centre}(t) - L_{B,centre}$ computed from the core region with $V_{centre} = (0.25H)^3$, where $L_{B,centre}(t)$ is the instantaneous, but volume averaged Bolgiano length scale and $L_{B,centre}$ the time and volume averaged Bolgiano length scale, for (*a*) $Pr = 0.7$ and (*b*) $Pr = 4.38$. $Ra = 1 \times 10^6$ (+), $Ra = 1 \times 10^7$ (○), $Ra = 1 \times 10^8$ (◇) and $Ra = 1 \times 10^9$ (▽).

of the scaling observed in our DNS is, however, one order of magnitude smaller than the experimental observation. We are not sure what causes this difference. We are confident that it is neither a result of the resolution, nor an effect of transient data, which in our experience lead to higher, but not to lower dissipation rates (which might be the case for $Ra = 3 \times 10^9$, where we started averaging only 300 time units after the initialization using a flow field with the same simulation parameters, but a lower resolution). There is, however, evidence that the temperature fluctuations scale very differently in a cylindrical and a cubic cell, which we suspect might be the reason for the difference. We will address the influence of the geometry in a subsequent publication.

We now ask the question of how the instantaneous Bolgiano length scales in the centre behave. For this purpose the p.d.f.s $P(\delta L_B)$ computed from the centre region are presented in figure 9. It is observed that $L_{B,centre}$ coincides with the most probable value of the local Bolgiano length scale, for all Ra and Pr investigated here. Comparison of $P(L_B)$ for $Ra = 1 \times 10^7$ and different Prandtl numbers reveals that the p.d.f. of the higher Prandtl number is much narrower than the one of the lower Prandtl number. It also becomes clear that for all Ra with $Pr = 0.7$ there is a fair probability of $\sim$5 % of observing a Bolgiano length scale that is of the size of the box. Since the probability of observing very large L_B is larger than the probability of observing very small L_B, the p.d.f. is positively skewed.

5. Energy balance

The globally averaged turbulent-kinetic-energy and temperature-variance dissipation rates obey the following exact relations:

$$Nu = \langle \epsilon_u \rangle_{global} (RaPr)^{1/2} + 1, \tag{5.1}$$

$$Nu = \langle \epsilon_T \rangle_{global} (RaPr)^{1/2}, \tag{5.2}$$

which are both equally valid and therefore hold at the same time. It is one of the key assumptions of the GL theory (Grossmann & Lohse 2000, 2004, 2011) that the global heat flux can be decomposed into contributions from the bulk and the boundary layers and it is therefore of key interest to verify this assumption. In order to answer the question of whether or not the local heat flux in the centre of the cell is balanced by the turbulent-kinetic-energy dissipation rate or the temperature-variance dissipation rate Ni *et al.* (2011) calculate the local vertical heat flux in the centre of the cell as

$$Nu_{centre} = \langle \epsilon_u \rangle_{centre} (RaPr)^{1/2}. \tag{5.3}$$

By comparing their data with direct heat flux measurements by Shang *et al.* (2004) they found that in the centre of their cylindrical cell the heat transfer is balanced by the turbulent-kinetic-energy dissipation rate, while previous experimental measurements in water (He *et al.* 2007; Shang *et al.* 2008) have shown that a balance of the form

$$Nu_{centre} = \langle \epsilon_T \rangle_{centre} (RaPr)^{1/2} \tag{5.4}$$

does not hold. It is, however, experimentally difficult to access all necessary quantities at the same time, in particular in gases. We therefore further test this observation by comparing the Nusselt numbers calculated through (5.3) and (5.4) with direct measurements of the local vertical heat flux for two different Pr in the centre of the cube. We compute the local Nusselt number as

$$Nu_{centre} \equiv (RaPr)^{1/2} \langle u_z T' \rangle_{t,centre} \tag{5.5}$$

using our non-dimensional set of variables (i.e. $Nu \equiv (\langle \hat{u}_z \hat{T}' \rangle_{t,centre})/(\hat{\kappa} \Delta \hat{T}/\hat{H})$ using dimensional quantities).

Figure 10 compares the directly measured vertical heat flux in the core region with the vertical heat flux calculated from the turbulent-kinetic-energy dissipation rate using (5.3) and the temperature-variance dissipation rate using (5.4) for both Prandtl numbers.

The results for $Pr = 0.7$ presented in figure 10(*a*) reveal that the local heat flux and the temperature-variance dissipation rate exhibit a similar scaling although their absolute values differ by almost one order of magnitude. Figure 10(*b*) for $Pr = 4.38$ illustrates that the directly measured heat flux and the heat flux calculated from (5.3)) match closely for $Ra \leqslant 5 \times 10^7$, which is in agreement with the findings by Ni *et al.* (2011), who observed that in their cylindrical cell filled with water the local vertical heat flux in the centre of the cell is balanced by the local turbulent-energy-dissipation rate. With increasing Ra, however, the two quantities extracted from the simulations begin to differ. This might be due to a lack of statistical data, which might prevent us from capturing very rare events, or a result of a different behaviour of the bulk flow in a cube as compared to a cylinder, as was for example observed by Daya & Ecke (2001). We therefore compare our results with experimental data obtained by Shang *et al.* (2004) in the centre of a cylindrical cell with $Ra \approx 10^9$ and $Pr = 5.5$. It can be seen from figure 11(*a*) that the numerical and the experimental data are in good agreement, even for values of the probability density as low as 10^{-5}. The only remaining parameter to explain the discrepancy is Nu_{rms} that has been used to normalize the p.d.f., implying that the dynamics of the bulk are different in a cube and a cylinder.

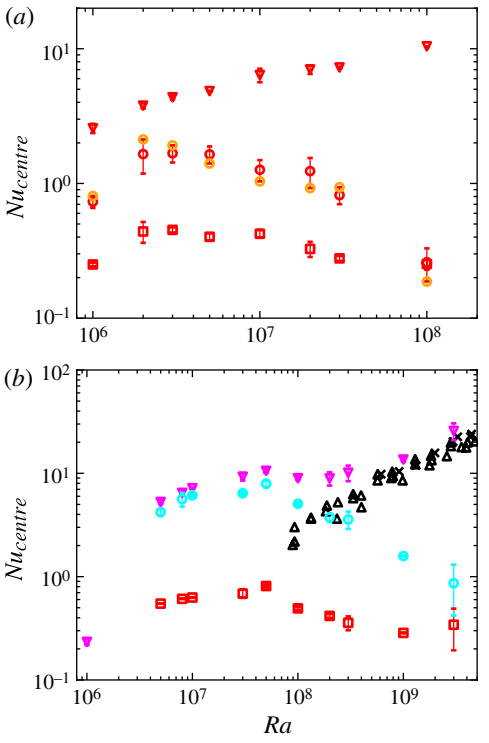

FIGURE 10. (Colour online) *Ra*-scaling of direct measurements of the local Nusselt number averaged over the entire time series (○), and the local Nusselt number estimated through (5.3) (▽) and (5.4) (□) all averaged over the volume $V_{centre} = (0.25H)^3$ for (*a*) $Pr = 0.7$ and (*b*) $Pr = 4.38$. Experimental data by Ni *et al.* (2011) (×) calculated from kinetic-energy dissipation rates, i.e. (5.3), and direct measurements of the local heat flux by Shang, Tong & Xia (2008) (△) are given in (*b*) for comparison.

The non-symmetric shape of the p.d.f. reflects the presence of two different phenomena in the bulk region: random fluctuations represented by the negative exponential tail of the p.d.f., while their positive tail is superimposed with increasingly intermittent fluctuations which carry a net heat flux through the bulk. In figure 11(*b*) we compare the p.d.f.s of the local heat flux averaged in time and over the core region for different Rayleigh and Prandtl numbers. It is observed that for the cases with higher Prandtl number the Nusselt number fluctuations are stronger, and hence the p.d.f. more skewed, implying that more heat is transported through the bulk at higher Prandtl numbers. This can be quantified by calculating the skewness of the p.d.f. We find that this skewness increases monotonically with *Ra* as can be seen from figure 12. Since the scaling of the skewness of the p.d.f.s shows a monotonic behaviour with *Ra*, we conclude that the effect of very rare events might not be as large as initially suspected, so that a geometrical effect appears to be the most plausible reason for the observed difference in experimental findings in cylindrical cells.

Comparing the p.d.f.s of the vertical heat transport through the bulk with the heat transport along the sidewall or through the entire cell, as measured experimentally by e.g. Shang, Tong & Xia (2005) and Gasteuil *et al.* (2007), it is evident that the Nusselt number fluctuations in the cell centre are about one order of magnitude

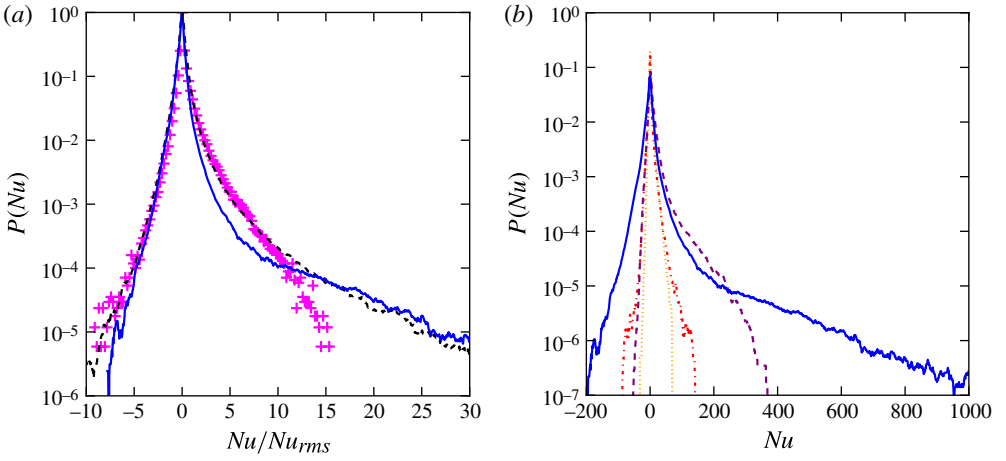

FIGURE 11. (Colour online) (*a*) Comparison of p.d.f.s of the local vertical heat flux measured in the core region of the flow for $Ra = 1 \times 10^9$, $Pr = 4.38$ (- -) and $Ra = 3 \times 10^9$, $Pr = 4.38$ (—) with experimental data by Shang *et al.* (2004) (+). (*b*) p.d.f.s of the local vertical heat flux for $Ra = 3 \times 10^6$, $Pr = 0.7$ (· · ·), $Ra = 1 \times 10^8$, $Pr = 0.7$ (-·-), $Ra = 1 \times 10^7$, $Pr = 4.38$ (- -) and $Ra = 3 \times 10^9$, $Pr = 4.38$ (—) all averaged in time and over the core region of the cube.

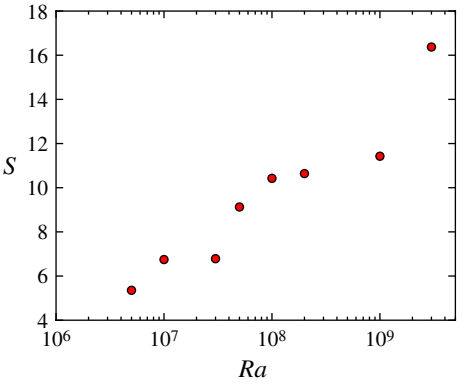

FIGURE 12. (Colour online) Skewness of the p.d.f.s of the local heat flux in the centre ($V_{centre} = (0.25H)^3$) of the cube for $Pr = 4.38$ (●).

smaller compared to the measurements that are subject to the frequent passing by of the thermal plumes.

In order to gain a deeper insight into the dynamics of the heat transfer processes in the core region of RBC, we evaluate the joint p.d.f. $P(\epsilon_u, \epsilon_T)$ of the turbulent-kinetic-energy dissipation rate and the temperature-variance dissipation rate and the conditional average $\langle Nu|\epsilon_u, \epsilon_T\rangle_{centre}$ of the local heat flux depending on ϵ_u and ϵ_T. The joint p.d.f.s of ϵ_u and ϵ_T presented in figure 13 reveal that, independent of Ra and Pr, the highest joint probability of ϵ_u and ϵ_T is found to occur at values smaller than their respective mean values, while high dissipation rates are rarely observed. It is, however, noted that there is a general tendency for high dissipation rates to occur together,

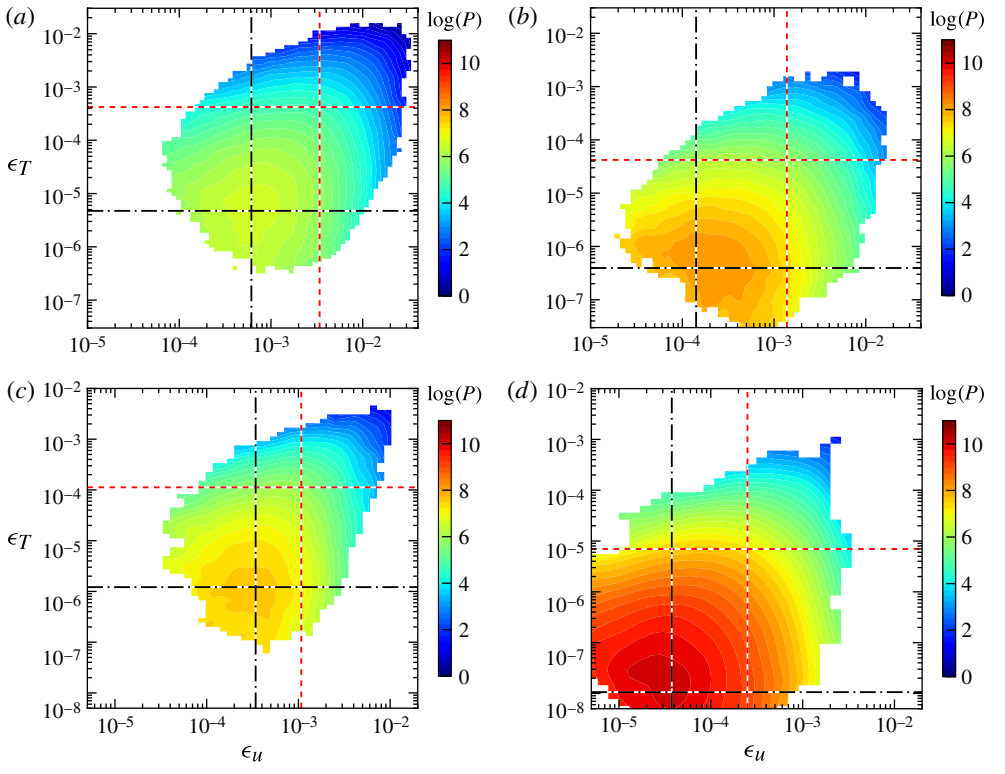

FIGURE 13. (Colour online) Joint p.d.f.s of ϵ_u and ϵ_T in the core region of the cube for (*a*) $Ra = 3 \times 10^6$, $Pr = 0.7$, (*b*) $Ra = 1 \times 10^8$, $Pr = 0.7$, (*c*) $Ra = 5 \times 10^6$, $Pr = 4.38$ and (*d*) $Ra = 1 \times 10^9$, $Pr = 4.38$. The colour scale is in $\log(P(\epsilon_u, \epsilon_T))$. The dashed red lines indicate the mean values of ϵ_u and ϵ_T averaged over the core region and the dot-dashed black lines their respective most probable values.

especially at $Pr = 4.38$, which can be seen from the protrusion in the top right corner, while events with only high ϵ_u or high ϵ_T are hardly observed. This demonstrates that few, but extreme events increase the dissipation rates in the bulk by around an order of magnitude.

The conditional average of the local heat flux in figure 14 shows that for both Prandtl numbers and all Rayleigh numbers the conditionally averaged heat flux is increasing from low to high dissipation rates. It appears that the highest values of the local heat flux occur for values of the dissipation rates larger than their mean, revealing that heat is primarily carried through the bulk by rare, but extreme events, which might be linked to the thermal plumes.

6. Structure functions in the core region

For sufficiently high Ra it is expected that for separations r within the inertial range the pth-order structure functions of velocity $S_p^u = \langle(|\Delta_r u'|)^p\rangle$ and (passively advected) temperature increments $S_p^T = \langle(|\Delta_r T'|)^p\rangle$ scale according to the K41 prediction, namely,

$$\langle(|\Delta_r u'|)^p\rangle = \beta_p \epsilon_u^{p/3}\, r^{p/3} \tag{6.1}$$

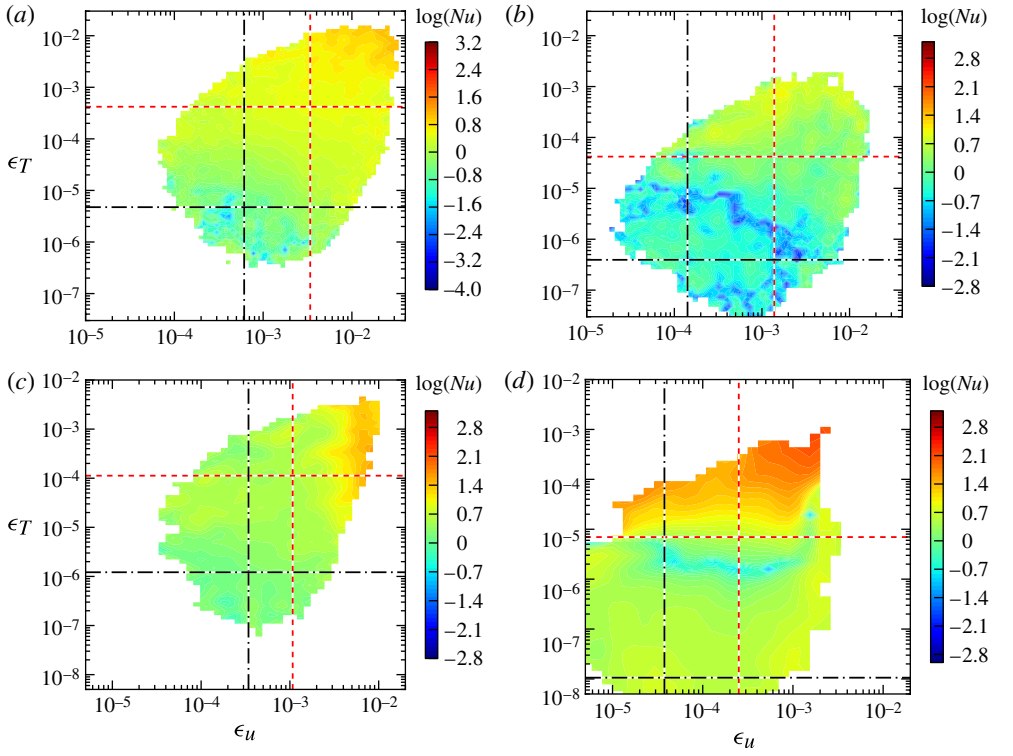

FIGURE 14. (Colour online) Local vertical heat flux $\langle Nu|\epsilon_u, \epsilon_T\rangle_{centre}$ in the core region of the cube, conditioned on the local turbulent-kinetic-energy dissipation rate ϵ_u and temperature-variance dissipation rate ϵ_T for (*a*) $Ra = 3 \times 10^6$, $Pr = 0.7$, (*b*) $Ra = 1 \times 10^8$, $Pr = 0.7$, (*c*) $Ra = 5 \times 10^6$, $Pr = 4.38$ and (*d*) $Ra = 1 \times 10^9$, $Pr = 4.38$. The dashed red lines indicate the mean values of ϵ_u and ϵ_T averaged over the core region and the dot-dashed black lines their respective most probable values.

and

$$\langle(|\Delta_r T'|)^p\rangle = \beta_{T,p}\epsilon_T^{p/2}\,\epsilon_u^{-p/6}\,r^{p/3}, \tag{6.2}$$

respectively, where β_p and $\beta_{T,p}$ are constants. For BO59-scaling in the inertial range one would expect scalings of the form

$$\langle(|\Delta_r u'|)^p\rangle = \beta_{Bo,u,p}\epsilon_T^{p/5} r^{3p/5} \tag{6.3}$$

and

$$\langle(|\Delta_r T'|)^p\rangle = \beta_{Bo,T,p}\epsilon_T^{2p/5} r^{p/5}. \tag{6.4}$$

In order to check which range of Ra is of interest, we compare the integral length scale as a measure for the upper bound and $10\eta_k$ as a lower bound of the inertial range with the local Bolgiano length scale. We compute the longitudinal and transverse correlation functions $f(r) = \langle w'(\boldsymbol{r}_0 + r\boldsymbol{e}_z)w'(\boldsymbol{r}_0)\rangle_{t,global}$ and $g(r) = \langle w'(\boldsymbol{r}_0 + r\boldsymbol{e}_x)w'(\boldsymbol{r}_0)\rangle_{t,global}$. The longitudinal integral length scale in the vertical direction is then given by $L_{11} = \int_0^\infty f(r)\,\mathrm{d}r$. The three length scales are illustrated in figure 15, from which it can be deduced that for $Pr = 4.38$ Rayleigh numbers larger than 3×10^8 will not satisfy the condition $10\eta_k < L_B < L$. Here we only

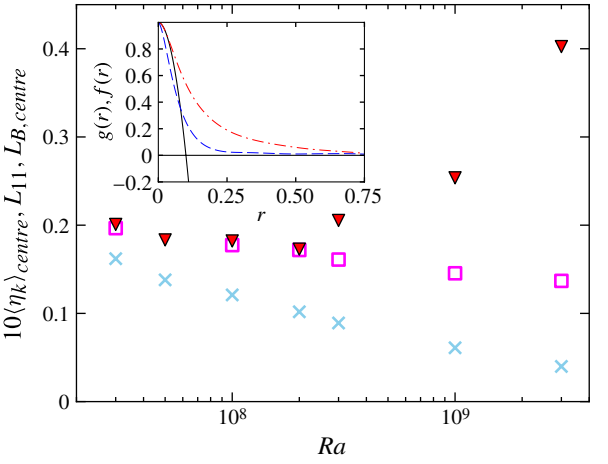

FIGURE 15. (Colour online) Ra-scaling of the integral length scale L_{11} (□), the local Bolgiano length scale $L_{B,centre}$ (▼) and $10\,\langle\eta_k\rangle_{centre}$ (×) for $Pr = 4.38$. The inset shows the longitudinal $f(r) = \langle w'(\boldsymbol{r}_0 + r\boldsymbol{e}_z)w'(\boldsymbol{r}_0)\rangle_{t,global}$ (- - -) and transverse correlation function $g(r) = \langle w'(\boldsymbol{r}_0 + r\boldsymbol{e}_x)w'(\boldsymbol{r}_0)\rangle_{t,global}$ (- -) of the vertical velocity for $Ra = 3 \times 10^8$ and $Pr = 4.38$ averaged over the whole volume. The parabola $1 + 2r^2/(f''(r = 0))$ (—) determining the Taylor microscale is given for reference.

plot the integral length scale computed from vertical velocity increments; however, using horizontal velocity increments, i.e. $f(r) = \langle u'(\boldsymbol{r}_0 + r\boldsymbol{e}_x)u'(\boldsymbol{r}_0)\rangle_{t,global}$, yields the same integral length scale. For some reason the structure functions for $Ra = 5 \times 10^7$ decay much more slowly to zero than for the neighbouring data points, leading to a significantly higher integral length scale, which is why we consider this point an outlier and do not plot it in the figure.

The longitudinal velocity structure functions averaged over the bulk region with $V = (0.5H)^3$ presented in figure 16(*a,c*) show that their inertial range is very short even for the highest Rayleigh number and no clear plateau is observed in the compensated plot. Due to the short inertial range of the structure functions on the one hand and the rapidly increasing local Bolgiano length scale on the other hand, it might not be possible to observe a transition from BO59 to K41 scaling in the core region of RBC with Prandtl numbers around unity by just examining the scaling of the structure functions. It is, however, noted that the longitudinal velocity increments in the vertical direction appear to approach a K41-like scaling. This observation is consistent with the results obtained by Sun *et al.* (2006), who found K41-scaling above the global Bolgiano length scale. The temperature structure functions in the vertical direction shown in figure 16(*b,d*), on the other hand, tend to approach a BO59 scaling for separations $r > L_{B,centre}$. However, it is also noted that for separations $r < L_{B,centre}$ the structure functions of vertical temperature increments exhibit a scaling exponent smaller than the BO59 one; it is approximately $p/10$.

We note that the separation of scales is not large enough to observe an r^0-scaling for separations $r > L_{11}$. We attribute this to the relatively large separation compared to the size of the container. Thus, for large separations r the structure function is no longer evaluated in the homogeneous region, but is influenced by the boundary layers. For larger Ra this effect should gradually vanish. Despite the short inertial range of the structure functions, the results seem to be consistent with K41 and BO59 scaling

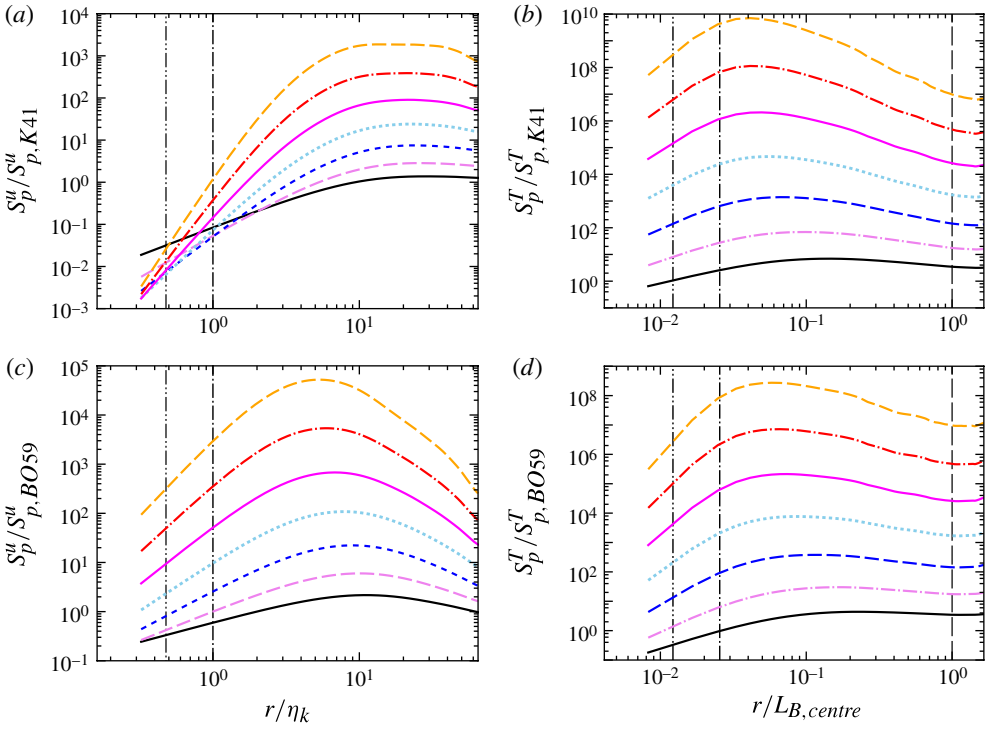

FIGURE 16. (Colour online) Plots of the pth-order longitudinal structure functions of the vertical velocity structure function compensated with (*a*) K41 and (*c*) BO59 scaling and temperature structure functions measured in the vertical direction in the centre of the cube compensated with (*b*) K41 and (*d*) BO59 scaling for $Ra = 1 \times 10^9$, $Pr = 4.38$; and (from bottom to top) $p = 2$ (—), $p = 3$ (-··-), $p = 4$ (- -), $p = 5$ (···), $p = 6$ (—), $p = 7$ (-··-), $p = 8$ (- -). The vertical lines represent the Batchelor length scale η_b (-···-), the Kolmogorov length scale (-··-) and the local Bolgiano length scales $L_{B,centre}$ (– –) averaged over the centre of the cube ($V_{centre} = (0.5H)^3$).

at scales $r > L_B$ of the longitudinal velocity and the temperature structure functions, respectively. An influence of the boundary layers on this region of the structure function can, however, not be ruled out.

We now analyse the mixed vertical velocity–temperature structure function $\langle \Delta w' \, \Delta T' \rangle$ and test whether the relation

$$\langle \Delta_r w' \, \Delta_r T' \rangle = \beta_{uT} \epsilon_T^{3/5} \, r^{4/5}, \tag{6.5}$$

where β_{uT} is the proportionality constant, derived from BO59 theory (see e.g. Benzi *et al.* 1998; Lohse & Xia 2010) holds for the turbulence in the core region of the cell. It is seen from figure 17 that the low-Prandtl-number cases do not follow the $r^{4/5}$-scaling suggested by theory, even though at $Ra = 1 \times 10^8$ and $Pr = 0.7$ there appears to be a small region that approaches the $r^{4/5}$-scaling. It is, however, questionable if this scaling will be more clearly visible at higher Ra, since the Bolgiano length scale is increasing rapidly and therefore possibly prevents observation of BO59 scaling in the mixed structure function at low Pr. At $Ra = 1 \times 10^9$ and $Pr = 4.38$ a small region with $r^{4/5}$-scaling has formed for $r > L_B$. It is noted that for this Prandtl number the local Bolgiano length scale is also increasing for $Ra \gtrapprox 3 \times 10^8$, so that increasing the

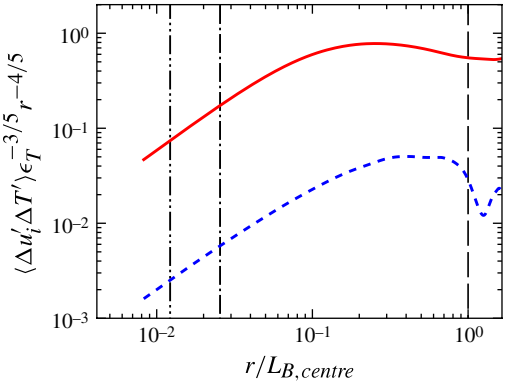

FIGURE 17. (Colour online) Compensated plots of the mixed vertical velocity–temperature structure function (—) and horizontal velocity–temperature structure function (- -) in the centre of the cube for $Ra = 1 \times 10^9$ and $Pr = 4.38$. The vertical lines represent the Batchelor length scale η_b (····), the Kolmogorov length scale (···) and the local Bolgiano length scales $L_{B,centre}$ (– –) averaged over the centre of the cube ($V_{centre} = (0.5H)^3$).

Rayleigh number might not be a good means to observe a longer range with BO59 scaling. On the other hand our data suggest that simulations at higher Prandtl numbers and moderate Rayleigh numbers will provide reasonably long inertial ranges following the BO59 scaling.

7. Conclusions

We have made a highly resolved DNS study of the small-scale properties of turbulent Rayleigh–Bénard convection in the core region of a cubic cell, with the Rayleigh number spanning approximately three decades and for two different values of the Prandtl number. We find that the *Ra*-scaling of the global Bolgiano length scale defined by the globally averaged dissipation rates can only be used as a scaling for sufficiently large *Pr*, when *Ra* is neither too high, nor too low. For $Pr = 4.38$ it is valid for $1\times10^7 \lessapprox Ra \lessapprox 2\times10^8$ and for $Pr = 0.7$ it is valid for $Ra \approx 1\times10^6$, suggesting that the region of applicability increases with increasing *Ra*. The complex scaling of the local Bolgiano length scale in the centre is a result of the different scaling behaviour of the temperature-variance dissipation rate and the turbulent-kinetic-energy dissipation rate at intermediate *Ra*.

The joint p.d.f. of the turbulent-kinetic-energy dissipation rate and the temperature-variance dissipation rate reveals that high values of ϵ_u and ϵ_T are very rare events in the bulk, but are likely to occur together. The joint most probable dissipation rates are on the other hand approximately one order of magnitude smaller than their respective mean values. This demonstrates that rare but extreme events have a significant influence on the dynamics of the bulk region. A conditional average of the local vertical heat flux depending on both turbulent-kinetic-energy dissipation rate and temperature-variance dissipation rate shows that the heat flux transported through the bulk increases as the local dissipation rate increases, where large values of the local vertical heat flux are predominant when the dissipation rates are larger than their mean, indicating that the heat carried by thermal plumes plays an important role in the dynamics of the bulk.

It is observed that for $Pr = 0.7$ the local vertical heat flux in the centre of RBC in a cube is balanced neither by the local temperature-variance dissipation rate nor by the local turbulent-kinetic-energy dissipation rate. However, the local vertical heat flux seems to obey the same scaling as the local temperature-variance dissipation rate. For $Pr = 4.38$ we observe that for $Ra \leqslant 3 \times 10^7$ the local vertical heat flux through the centre of the cell is balanced by the local turbulent-kinetic-energy dissipation rate, which agrees with the finding by Ni *et al.* (2011) observed for $5 \times 10^8 \leqslant Ra \leqslant 10^{10}$. Despite the fact that the numerically and experimentally measured normalized p.d.f.s of the local heat flux are in excellent agreement, our data do not confirm this observation for high Ra. This discrepancy needs to be further investigated and more statistical data should be collected in order to rule out long-term effects that might influence the normalization Nu_{rms}. However, since the skewness of the p.d.f.s is increasing with Ra, we infer that the differences observed here are an effect of the cubic geometry as opposed to the cylindrical geometry of the experiments. Based on the low-Ra data, we put forward the hypothesis that the balance of the local vertical heat flux in the centre of RBC is Prandtl-number dependent, which is balanced by the temperature-variance dissipation rate at low Pr and by the turbulent-kinetic-energy dissipation rate at high Pr.

Our results show that the inertial-range longitudinal velocity structure functions in the centre of the cube approach K41-scaling, while the temperature structure functions approach the BO59-scaling for $r > L_{B,centre}$. For smaller separations r the temperature structure functions exhibit a scaling $p/10$. These observations tend to be more clear and pronounced at high Prandtl numbers, suggesting further investigation of BO59 properties at high Pr. For the highest Ra simulated here we observe a tendency to follow the 4/5-power law of the mixed vertical velocity temperature structure function, which for $Ra = 1 \times 10^9$ and $Pr = 4.38$ forms a short 4/5 scaling at separations $r > L_{B,centre}$.

Acknowledgements

This work is supported in part by the Hong Kong Research Grants Council (RGC) under Grant No. CUHK 404409, in part by a RGC Direct Grant (project code: 2060441) and in part by the NSFC/RGC Joint Research Scheme under Grant No. N_CUHK462/11. M.K. acknowledges financial support by the EU Science and Technology Fellowship Programme China. This research was conducted using the resources of the Chinese University of Hong Kong's Information and Technology Service Centre and the High Performance Cluster Computing Centre, Hong Kong Baptist University, which receives funding from Research Grant Council, University Grant Committee of the HKSAR and Hong Kong Baptist University and the Leibnitz Rechenzentrum Munich.

REFERENCES

AHLERS, G., GROSSMANN, S. & LOHSE, D. 2009 Heat transfer and large-scale dynamics in turbulent Rayleigh–Bénard convection. *Rev. Mod. Phys.* **81** (2), 503–537.

BENZI, R., TOSCHI, F. & TRIPICCIONE, R. 1998 On the heat transfer in Rayleigh–Bénard systems. *J. Stat. Phys.* **93** (3/4).

BOFFETTA, G., DE LILLO, F., MAZZINO, A. & MUSACCHIO, S. 2012 Bolgiano scale in confined Rayleigh–Taylor turbulence. *J. Fluid Mech.* **690**, 426–440.

BOLGIANO, R. 1959 Turbulent spectra in a stably stratified atmosphere. *J. Geophys. Res.* **64** (12), 2226–2229.

CALZAVARINI, E., TOSCHI, F. & TRIPICCIONE, R. 2002 Evidences of Bolgiano scaling in 3D Rayleigh–Bénard convection. *Phys. Rev.* E **66**, 016304.

CHILLÀ, F. & SCHUMACHER, J. 2012 New perspectives in turbulent Rayleigh–Bénard convection. *Eur. Phys. J.* E **35** (58).

DAYA, Z. A. & ECKE, R. E. 2001 Does turbulent convection feel the shape of the container? *Phys. Rev. Lett.* **87** (18), 184501.

FUNFSCHILLING, D., BROWN, E., NIKOLAENKO, A. & AHLERS, G. 2005 Heat transport by turbulent Rayleigh–Bénard convection in cylindrical samples with aspect ratio one and larger. *J. Fluid Mech.* **536**, 145–154.

GASTEUIL, Y., SHEW, W. L., GIBERT, M., CHILLÀ, F., CASTAING, B. & PINTON, J.-F. 2007 Lagrangian temperature, velocity, and local heat flux measurement in Rayleigh–Bénard convection. *Phys. Rev. Lett.* **99** (234302).

GROSSMANN, S. & LOHSE, D. 2000 Scaling in thermal convection: a unifying theory. *J. Fluid Mech.* **407**, 27–56.

GROSSMANN, S. & LOHSE, D. 2004 Fluctuations in turbulent Rayleigh–Bénard convection: the role of plumes. *Phys. Fluids* **16** (12), 4462–4472.

GROSSMANN, S. & LOHSE, D. 2011 Multiple scaling in the ultimate regime of thermal convection. *Phys. Fluids* **23**, 045108.

HE, X., TONG, P. & XIA, K.-Q. 2007 Measured dissipation field in turbulent Rayleigh–Bénard convection. *Phys. Rev. Lett.* **98** (14), 144501.

KACZOROWSKI, M., SHISHKIN, A., SHISHKINA, O. & WAGNER, C. 2008 *New Results in Numerical and Experimental Fluid Mechanics VI*, vol. 96, pp. 381–388. Springer.

KUNNEN, R. P. J., CLERX, H. J. H., GEURTS, B. J., BOKHOVEN, L. J. A., VAN, AKKERMANS, R. A. D. & VERZICCO, R. 2008 Numerical and experimental investigation of structure-function scaling in turbulent Rayleigh–Bénard convection. *Phys. Rev.* E **77**, 016302.

LOHSE, D. & XIA, K.-Q. 2010 Small-scale properties of turbulent Rayleigh–Bénard convection. *Annu. Rev. Fluid Mech.* **42**, 335–364.

NI, R., HUANG, S.-D. & XIA, K.-Q. 2011 Local energy dissipation rate balances local heat flux in the centre of turbulent thermal convection. *Phys. Rev. Lett.* **107**, 174503.

SHANG, X.-D., QIU, X.-L., TONG, P. & XIA, K.-Q. 2004 Measurements of the local convective heat flux in turbulent Rayleigh–Bénard convection. *Phys. Rev.* E **70**, 026308.

SHANG, X.-D., TONG, P. & XIA, K.-Q. 2005 Test of steady-state fluctuation theorem in turbulent Rayleigh–Bénard convection. *Phys. Rev.* E **72**, 015301.

SHANG, X.-D., TONG, P. & XIA, K.-Q. 2008 Scaling of the local convective heat flux in turbulent Rayleigh–Bénard convection. *Phys. Rev. Lett.* **100**, 244503.

SHISHKINA, O., SHISHKIN, A. & WAGNER, C. 2009 Simulation of turbulent thermal convection in complicated domains. *J. Comput. Appl. Maths* **226**, 336–344.

SHISHKINA, O., STEVENS, R. J. A. M., GROSSMANN, S. & LOHSE, D. 2010 Boundary layer structure in turbulent thermal convection and consequences for the required numerical resolution. *New J. Phys.* **12**, 075022.

SUN, C., ZHOU, Q. & XIA, K.-Q. 2006 Cascades of velocity and temperature fluctuations in buoyancy-driven thermal turbulence. *Phys. Rev. Lett.* **97**, 144504.

WAGNER, S., SHISHKINA, O. & WAGNER, C. 2012 Boundary layers and wind in cylindrical Rayleigh–Bénard cells. *J. Fluid Mech.* **697**, 336–366.

XIA, K.-Q., LAM, S. & ZHOU, S.-Q. 2002 Heat-flux measurement in high-Prandtl-number turbulent Rayleigh–Bénard convection. *Phys. Rev. Lett.* **88** (6), 064501.

ZHOU, Q., SUN, C. & XIA, K. Q. 2008 Experimental investigation of homogeneity, isotropy, and circulation of the velocity field in buoyancy-driven turbulence. *J. Fluid Mech.* **598**, 361–372.